ISSN 1349-1113
JAXA-RR-05-013E

JAXA Research and Development Report

Feasibility Study for Precise Lunar Landing using SELENE-B Lander Configuration

Yoshiro HAMADA, Tetsujiro NINOMIYA, Yasuhiro KATAYAMA,
Yasuo SHINOMIYA, Kohtaro MATSUMOTO, Masayuki YAMAMOTO,
Shujiro SAWAI, Seiya UENO and Kentaro HAYASHI

December 2005

Japan Aerospace Exploration Agency

JAXA-RR-05-013E

JAXA Research and Development Report

Feasibility Study for Precise Lunar Landing using SELENE-B Lander Configuration

Yoshiro HAMADA, Tetsujiro NINOMIYA, Yasuhiro KATAYAMA, Yasuo SHINOMIYA,
Kohtaro MATSUMOTO, Masayuki YAMAMOTO, Shujiro SAWAI,
Seiya UENO and Kentaro HAYASHI

Advanced Space Technology Research Group
Institute of Aerospace Technology

December 2005

Japan Aerospace Exploration Agency

Feasibility Study for Precise Lunar Landing using SELENE-B Lander Configuration

Yoshiro HAMADA *1, Tetsujiro NINOMIYA *1, Yasuhiro KATAYAMA *1,
Yasuo SHINOMIYA *1, Kohtaro MATSUMOTO *1, Masayuki YAMAMOTO *1,
Shujiro SAWAI *1, Seiya UENO *2 and Kentaro HAYASHI *3

ABSTRACT

This paper concerns the evaluation of a guidance and control system for lunar landing. The lander, which is supposed to have the same configuration of SELENE-B (SELenological and ENgineering Explorer-B), is required to land precisely at a site where there are scientifically important features, with minimal fuel consumption while avoiding surface obstacles such as rocks and small craters which might jeopardize the landing. The guidance and control system are designed for this aim, and the feasibility of the landing is tested by Monte Carlo simulation. The results, however, indicated that the original configuration and landing sequence are not appropriate for precise and safe landing. Therefore, based on the results, the configuration and landing sequence are modified and tested by Monte Carlo simulation again.

Keywords : Guidance and Control, Lunar Lander, SELENE-B, Monte Carlo Simulation

要　約

本論文は，月面精密着陸に必要な誘導制御則について論ずる。取り扱う月面軟着陸機は，以前提案されていたSELENE-B（月軟着陸実験計画）と同じ構成を持つと仮定する。着陸機は，岩石や小さなクレータ等の危険な場所を避けつつ，科学的に意義のある地点へ精密に着陸することが要求される。本稿では，これを満足する着陸誘導制御則を設計し，モンテカルロシミュレーションによって評価を行なう。SELENE-Bと同じ構成及び着陸シーケンスでは，安全かつ精密な着陸は難しいことをシミュレーションで示し，その結果を受けて構成等に変更を加え，更なるシミュレーションで精密着陸の成立性を検証する。

1. Introduction

The moon is recognized as an important destination for space science and exploration [1]. The National Aeronautics and Space Administration (NASA) has presented a new policy [2] for space exploration that includes human expedition to the lunar surface. The European Space Agency (ESA) and other agencies have also planned to send spacecraft to the moon and some of these projects are now in progress [3].

The Japan Aerospace Exploration Agency (JAXA) released its long-term vision called "JAXA Vision" [4] in March 2005, in which the development and demonstration of technologies for lunar exploration will be achieved within about 10 years. JAXA will launch Japan's first large lunar orbiter, SELENE (SELenological and ENgineering Explorer), in 2007 [5], and a lunar landing mission which aims to send an unmanned lander to the lunar surface is being studied as a follow-on mission [6]. The lander is required to land precisely at a site that has scientifically

*　平成17年11月7日受付（received 7 November, 2005）

*1 Japan Aerospace Exploration Agency (JAXA)

*2 Yokohama National University

*3 Mitsubishi Space Software Co., LTD.

interesting features. This may be, however, impossible if there are obstacles such as large rocks and small craters that prevent a safe landing there. Therefore, the lander is required to find an obstacle-free area as close as possible to the original target site and to land there safely. A major technical research subject of the mission is thus the development of technology to achieve this.

This paper is concerned with a guidance and control system for precise and safe landing. The amount of fuel that can be carried is strictly limited due to mission payload constraints. Thus, a guidance strategy that minimizes fuel consumption is essential. The guidance and control system is designed for this aim, and the feasibility of the landing is tested by Monte Carlo simulation, which is often used to evaluate the robustness of flight systems against various uncertainties. Monte Carlo simulation is able to evaluate nonlinear systems directly, and its results reflect the influences of various combinations of uncertain parameters. Firstly we show the results of the simulation using the "SELENE-B" configuration and the landing sequence studied in 2002. The results make it clear that the original configuration and the landing sequence are not appropriate for precise and safe landing. And then the simulation results using the modified configuration are shown.

This paper is organized as follows. The original configuration and landing sequence of "SELENE-B" are described in Section 2. The proposed guidance and control system is presented in Section 3. Section 4 shows the Monte Carlo simulation results using the original configuration. Based on the results, we modify the configuration and landing sequence with which we show the simulation results in Section 5.

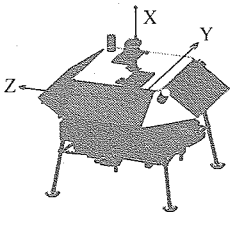

Figure 1: Conceptual design of the lunar lander and its body-fixed coordinates (From "proposal of the SELENE-B mission" [6]).

Notation

ϕ, θ, ψ: attitude angles
P, Q, R: angular velocities
T_r, T_p, T_y: RCS torques
T: main engine thrust
m: mass of the lander
m_e: estimated mass
u_T: thrust duty cycle
$Ton_{\min}$: minimum on-time of the main engine
$Toff_{\min}$: minimum off-time of the main engine
I_{SP}: specific impulse of the main engine
g: gravitational acceleration
g_m: gravitational acceleration on the moon (assumed to be a constant)
$\{\cdot\}^l$: a state variable defined in the lunar local coordinates
$\{\cdot\}^b$: a state variable defined in the body-fixed coordinates
$\{\cdot\}^g$: a state variable defined in the reference trajectory coordinates
$\{\cdot\}_a$: a command output from the guidance system
$\{\cdot\}_r$: a state variable of the reference trajectory

2. Preliminaries

2.1 Configuration of the Lander

The lunar lander considered here is shown in Figure 1. It is equipped with twelve reaction control system (RCS) thrusters for attitude control and a 1,700N main thruster. The attitude of the lander around each axis is always controlled by two pairs of RCS thruster (one pair for the plus direction and the other for the minus direction) in order to generate a "pure" torque without a linear force. Since it has no direct translation control force in the horizontal plane, the lander must tilt to use the resulting sideways

Table 1: Major lander characteristics.

Initial mass	600[kg]
Initial descending velocity (after de-orbit)	-40[m/sec]
Roll inertia moment	228.2[kgm^2]
Pitch inertia moment	170.1[kgm^2]
Yaw inertia moment	168.9[kgm^2]
Main thrust	1,700[N]
Main thrust ISP	316[sec]
Maximum RCS thrust (per one thruster)	40[N]
Length of RCS moment arm	1[m]
RCS ISP	280[sec]

component of engine thrust to control horizontal velocity. The major characteristics of the lander are shown in Table 1.

2.2 Landing Sequence

The landing sequence after de-orbit is divided into the following two phases: a powered descent phase during which the lander cancels its large horizontal velocity, and a vertical descent phase (below 3,500m altitude) during which the lander must detect and avoid obstacles on the lunar surface. This paper deals with only the vertical descent phase. The landing sequence of the vertical descent phase is divided into the following five subphases considering the performance of the imaging sensor used for obstacle detection.

- Initial error accommodation (3,500m-500m altitude): Navigation error accumulated during de-orbit is accommodated in this subphase. The maximum necessary shift in horizontal position is estimated to be 500m.
- Rough obstacle avoidance (500 m-100m): Larger obstacles can be detected at an altitude of 500m. During this subphase, the lander moves to a safe landing location to avoid large obstacles. A maximum horizontal shift of 250m is assumed.
- Precise obstacle avoidance (100m-10m): During this subphase, the lander avoids smaller obstacles detected from an altitude of 100m. A maximum horizontal shift of 75m is assumed. Considering the final freefall subphase, the descent velocity at the end of this subphase is set at around 1.5m/sec.
- Constant speed descent (10m-2m): This subphase is introduced in consideration of altitude navigation error. The lander descends vertically at a constant speed of around 1.5m/sec in order to avoid crashing into the lunar surface.
- Freefall (2m-0m): To avoid stirring up lunar surface material (regolith) by using the main thruster near the surface, the main thruster is stopped at an altitude of 2m and the lander then freefalls to the surface. If the descent speed at main thruster cut-off is around 1.5m/sec, the lander will touch down within about 2 seconds at a vertical speed of about 3 m/s, which is within the limits of the vehicle's undercarriage.

2.3 Navigation System

The navigation system in this paper comprises an inertial measurement unit (IMU), a radio altimeter/velocimeter (RA/RV), and a Kalman navigation filter. The RA/RV can operate down to 30m altitude. The outputs of the IMU and RA/RV are integrated, and position, velocity, and attitude errors are estimated by the Kalman filter. These estimated state variables are used by the guidance and control system. Details of the navigation system have been published in previous papers [6][7].

2.4 Obstacle Detection System

Obstacles on the lunar surface are detected using a stereo imaging sensor. At the start of the rough obstacle avoidance and precise obstacle avoidance subphases, the obstacle detection system senses large rocks and small craters below the lander which may endanger landing, and identifies an obstacle-free area wide enough for landing in the neighborhood of the original target site. The objective point of each subphase, to which the guidance and control system guides the lander, is set to exactly above the center of the obstacle-free area. The system is activated only when the main thruster is not firing in order to avoid flaer's influence over the stereo imaging sensor.

2.5 Coordinate Systems

A number of coordinate systems are used in this paper. Conversion between these coordinate systems is accomplished by transformation matrices.

2.5.1 Lunar Local Coordinates

Assuming the curvature of the lunar surface around the target site to be negligible, a lunar local coordinate system is defined as follows:

- x^l: a vertical unit vector pointing downward the lunar surface.
- y^l: a unit vector pointing east.
- z^l: a unit vector pointing north.

Its origin is the projection of the initial position of the lander at the start of the current subphase to the lunar surface. A vector in lunar local coordinates is denoted with a superscript l.

2.5.2 Body-Fixed Coordinates

A body-fixed coordinate system is defined as shown in Figure 1. Its origin is at lander's center of mass. A vector in body-fixed coordinates r^b is transformed to a vector in lunar local coordinates r^l by the following transformation matrix C_b^l:

$$r^l = C_b^l(\phi,\theta,\psi)r^b, \tag{1}$$

$$C_b^l = \begin{bmatrix} c\theta c\psi & -c\theta s\psi & s\theta \\ s\phi s\theta c\psi + c\phi s\psi & -s\phi s\theta s\psi + c\phi c\psi & -s\phi c\theta \\ -c\phi s\theta c\psi + s\phi s\psi & c\phi s\theta s\psi + s\phi c\psi & c\phi c\theta \end{bmatrix},$$

$$(s* := \sin*,\ c* := \cos*),$$

where ϕ, θ and ψ denote the roll, pitch and yaw angles of the lander respectively.

2.5.3 Target Attitude Coordinates

The target attitude coordinate system is the body-fixed coordinate system at the target attitude. It is defined using the target attitude angles which are calculated by the guidance system and denoted as ϕ_a, θ_a and ψ_a. A vector in this coordinate is expressed with a superscript a. The transformation matrix C_a^l (ϕ_a, θ_a, ψ_a) is defined in the same way as C_b^l.

2.5.4 Reference Trajectory Coordinates

The guidance system reference trajectory is determined in a plane normal to the lunar surface and includes the initial point and objective points of the lander in the current subphase. This coordinate system is defined in order to generate the reference trajectory. Its origin is the projection of the initial point of the current subphase to the lunar surface. The x axis is the same direction of x^l, the y axis points towards the projection of the objective point to the lunar surface, and the z axis is defined to make a right-handed coordinate system. State variables in the reference trajectory coordinate system are shown with a superscript g. This coordinate system is transformed to the lunar local coordinate system using the transformation matrix C_g^l, which is calculated using the initial position (y_i^l, z_i^l) and final position (y_f^l, z_f^l) of the lander in the lunar coordinate system:

$$C_g^l(\phi_g) = \begin{bmatrix} 1 & 0 & 0 \\ 0 & \cos\phi_g & -\sin\phi_g \\ 0 & \sin\phi_g & \cos\phi_g \end{bmatrix}, \tag{2}$$

$$\text{where } \phi_g = \tan^{-1}\left(\frac{z_f^l - z_i^l}{y_f^l - y_i^l}\right). \tag{3}$$

3. Guidance and Control System

3.1 Overview

The guidance and control system of the lander consists of six modules:

- subphase management
- reference trajectory generation
- guidance to the reference trajectory
- main thrust modulation
- attitude control
- mass estimation

Figure 2 depicts the relationships among these modules. The basic concept of the system is as follows [8]. At the start of each subphase, the objective point at the end of the subphase is decided by the obstacle detection system, and the reference trajectory to the point is calculated so as to minimize fuel consumption during the landing sequence. Then, during the subphase, attitude and thrust are controlled so that the lander follows the reference trajectory. The function of each module is explained briefly in the following subsections.

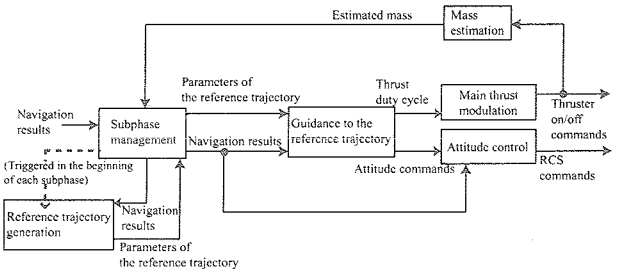

Figure 2: Guidance and control system modules.

3.2 Subphase Management

This module supervises the current subphase in the landing sequence and the current state parameters (position, velocity, attitude, etc.) estimated by the navigation system. The subphase is determined by current altitude (see section 2.2). When the subphase changes, this module invokes the reference trajectory generation module to obtain the calculated reference trajectory parameters.

The subphase management module also counts elapsed time from the start of the current subphase, which is used in the guidance to the reference trajectory module.

3.3 Reference Trajectory Generation

The reference trajectory is determined as the minimum fuel trajectory from the initial point to the objective point of the current subphase. It is determined in the reference trajectory coordinate system, which helps to reduce the amount of computation required.

For each subphase, the initial state and final position are input to this module, whereas the module can choose the final velocity. Although the reference trajectory is designed to optimize fuel consumption, it is desirable to reduce the amount of computation required to allow the algorithm to be implemented in the lander, and so a number of simplifying assumptions are made. Firstly, the thruster can generate arbitrary thrust up to the maximum thrust. Since thrust (T) is always divided by mass (m) in the equations of motion, T/m is treated as one variable ($=a$) and assumed not to change during a subphase. This simplification helps to solve the optimization problem easily. Secondly, the attitude angle in reference trajectory coordinates is assumed to be fixed at Ψ during the horizontal acceleration, and at $-\Psi$ during horizontal deceleration. The attitude angle is limited up to $\bar{\Psi}$, and the attitude angle ratio is set to be maximum value ($\pm\bar{\omega}$) so that the lander can follow the reference trajectory. In this study we set:

$$\bar{\Psi} = 30[\mathrm{deg}],$$
$$\bar{\omega} = 5.0[\mathrm{deg/sec}].$$

3.3.1 Coordinate transformation

As is mentioned in the previous section, the reference trajectory is defined in the reference trajectory coordinate system. Since the subphase management module uses the lunar local coordinate system, it is necessary to apply a coordinate transformation to the initial position ($*_i$), initial velocity (v_{*i}) and final position ($*_f$) of the current subphase:

$$\begin{bmatrix} x_i^g \\ y_i^g \\ z_i^g \end{bmatrix} = C_l^g \begin{bmatrix} x_i^l - 0 \\ y_i^l - y_i^l \\ z_i^l - z_i^l \end{bmatrix} = \begin{bmatrix} x_i^l \\ 0 \\ 0 \end{bmatrix}, \tag{4}$$

$$\begin{bmatrix} v_{xi}^g \\ v_{yi}^g \\ v_{zi}^g \end{bmatrix} = C_l^g \begin{bmatrix} v_{xi}^l \\ v_{yi}^l \\ v_{zi}^l \end{bmatrix}, \tag{5}$$

$$\begin{bmatrix} x_f^g \\ y_f^g \\ z_f^g \end{bmatrix} = C_l^g \begin{bmatrix} x_f^l - 0 \\ y_f^l - y_i^l \\ z_f^l - z_i^l \end{bmatrix}, \tag{6}$$

$$(C_l^g = \{C_g^l\}^{-1})$$

Since all state variables concerned with this module are defined in the reference trajectory coordinate system, the superscript g is omitted in the following sections for simplicity.

3.3.2 Reference Trajectory generation

There are two types of candidate trajectory for the reference trajectory.

Type 1: horizontal acceleration and deceleration
Type 2: horizontal deceleration only

Although the former type of trajectory can move the lander to a farther area regardless of the initial horizontal velocity, some time is necessary to change the lander's attitude to alter the horizontal thrust component to accelerate and decelerate. As a result, this trajectory has an unreachable area which can actually be reached with shorter time acceleration. The latter type of trajectory allows this unreachable area to be covered.

Trajectory type 1: horizontal acceleration and deceleration At the start of the subphase, the lander is in freefall (t_{f1} sec). It then accelerates (t_a sec) and decelerates (t_d sec) horizontally.

Step 1: Freefall ($t \le t_{f1}$)

The lander freefalls for t_{f1} seconds. This step is necessary since the main thruster should not fire in the beginning of the subphase in order to activate the obstacle detection system. During this step, the reference trajectory is expressed as follows.

$$\psi_r(t) = 0,$$
$$R_r(t) = 0,$$
$$v_{x,r}(t) = v_{xi} - g_m t,$$
$$v_{y,r}(t) = v_{yi},$$
$$x_r(t) = x_i + v_{xi}t - \frac{1}{2}g_m t^2,$$
$$y_r(t) = y_i + v_{yi}t,$$

where

$\psi_r(t)$: reference angle,
$R_r(t)$: reference rate,
$v_{x,r}(t)$, $v_{y,r}(t)$: reference velocity,
$x_r(t)$, $y_r(t)$: reference position,
(in the reference trajectory plane).

Step 2: Transition to horizontal acceleration ($t_{f1} \le t \le t_{f1} + \delta t$, where $\delta t = \frac{|\Psi|}{\bar{\omega}}$)

The lander changes its attitude with constant angular velocity $\bar{\omega}$ [rad/sec] until it turns to Ψ [rad]. Let x_k, y_k, v_{xk}, v_{yk} be the position and velocity at the end of the k-th step, and τ_k be the elapsed time in the k-th step (*e.g.* $\tau_2 = t - t_{f1}$). Then the reference trajectory is expressed as follows:

$$R_r(\tau_2) = s_1\bar{\omega},$$

$$v_{x,r}(\tau_2) = v_{x1} - g_m\tau_2 + \frac{a}{\bar{\omega}}\sin\bar{\omega}\tau_2,$$

$$v_{y,r}(\tau_2) = v_{y1} + \frac{as_1}{\bar{\omega}}(1-\cos\bar{\omega}\tau_2),$$

$$x_r(\tau_2) = x_1 + v_{x1}\tau_2 - \frac{1}{2}g_m\tau_2^2 + \frac{a}{\bar{\omega}^2}(1-\cos\bar{\omega}\tau_2),$$

$$y_r(\tau_2) = y_1 + \left(v_{y1} + \frac{as_1}{\bar{\omega}}\right)\tau_2 - \frac{as_1}{\bar{\omega}^2}\sin\bar{\omega}\tau_2,$$

where

$$s_1 = \mathrm{sign}(\Psi),$$
$$a = \frac{T}{m} = \frac{T_{\max}u_T}{m} = \alpha\cdot I_{SP}\cdot g.$$

Step 3: Horizontal acceleration ($t_{f1} + \delta t \le t \le t_{f1} + \delta t + t_a$)

The lander accelerates for t_a seconds.

$$\psi_r(\tau_3) = \Psi,$$
$$R_r(\tau_3) = 0,$$
$$v_{x,r}(\tau_3) = v_{x2} + (a\cos\Psi - g_m)\tau_3,$$
$$v_{y,r}(\tau_3) = v_{y2} + as_1\sin|\Psi|\tau_3,$$
$$x_r(\tau_3) = x_2 + v_{x2}\tau_3 + \frac{1}{2}(a\cos\Psi - g_m)\tau_3^2,$$
$$y_r(\tau_3) = y_2 + v_{y2}\tau_3 + \frac{1}{2}as_1\sin|\Psi|\tau_3^2,$$
$$(\tau_3 = t - t_{f1} - \delta t).$$

Step 4: Transition to horizontal deceleration ($t_{f1} + \delta t + t_a \le t \le t_{f1} + 3\delta t + t_a$)

To decelerate, the lander changes its attitude with constant angular velocity $-\bar{\omega}$ [rad/sec] until it turns to $-\Psi$.

$$\psi_r(\tau_4) = s_1(|\Psi| - \bar{\omega}\tau_4),$$
$$R_r(\tau_4) = -s_1\bar{\omega},$$
$$v_{x,r}(\tau_4) = v_{x3} - g_m\tau_4 - \frac{a}{\bar{\omega}}\{\sin(|\Psi| - \bar{\omega}\tau_4) - \sin|\Psi|\},$$
$$v_{y,r}(\tau_4) = v_{y3} + \frac{as_1}{\bar{\omega}}\{\cos(|\Psi| - \bar{\omega}\tau_4) - \cos|\Psi|\},$$
$$x_r(\tau_4) = x_3 + \left(v_{x3} + \frac{a}{\bar{\omega}}\sin|\Psi|\right)\tau_4 - \frac{1}{2}g_m\tau_4^2 - \frac{a}{\bar{\omega}^2}\{\cos(|\Psi| - \bar{\omega}\tau_4) - \cos|\Psi|\},$$
$$y_r(\tau_4) = y_3 + \left(v_{y3} - \frac{as_1}{\bar{\omega}}\cos|\Psi|\right)\tau_4 - \frac{as_1}{\bar{\omega}^2}\{\sin(|\Psi| - \bar{\omega}\tau_4) - \sin|\Psi|\},$$
$$(\tau_4 = t - t_{f1} - \delta t - t_a).$$

Step 5: Horizontal deceleration ($t_{f1} + 3\delta t + t_a \le t \le t_{f1} + 3\delta t + t_a + t_d$)

The lander decelerates for t_d seconds.

$$\psi_r(\tau_5) = -\Psi,$$
$$R_r(\tau_5) = 0,$$
$$v_{x,r}(\tau_5) = v_{x4} + (a\cos\Psi - g_m)\tau_5,$$
$$v_{y,r}(\tau_5) = v_{y4} - as_1\sin|\Psi|\tau_5,$$
$$x_r(\tau_5) = x_4 + v_{x4}\tau_5 + \frac{1}{2}(a\cos\Psi - g_m)\tau_5^2,$$
$$y_r(\tau_5) = y_4 + v_{y4}\tau_5 - \frac{as_1}{2}\sin|\Psi|\tau_5^2,$$
$$(\tau_5 = t - t_{f1} - 3\delta t - t_a).$$

Step 6: Transition to the next subphase ($t_{f1} + 3\delta t + t_a + t_d \le t \le t_{f1} + 4\delta t + t_a + t_d$)

The lander stops decelerating and returns to a vertical attitude with constant angular velocity $-\bar{\omega}$ [rad/sec].

$$\psi_r(\tau_6) = -s_1(|\Psi| - \bar{\omega}\tau_6)$$
$$R_r(\tau_6) = s_1\bar{\omega},$$
$$v_{x,r}(\tau_6) = v_{x5} - g_m\tau_6 - \frac{a}{\bar{\omega}}(\sin(|\Psi| - \bar{\omega}\tau_6) - \sin|\Psi|)$$
$$v_{y,r}(\tau_6) = v_{y5} - \frac{as_1}{\bar{\omega}}\{\cos(|\Psi| - \bar{\omega}\tau_6) - \cos|\Psi|\}$$
$$x_r(\tau_6) = x_5 + \left(v_{x5} + \frac{a}{\bar{\omega}}\sin|\Psi|\right)\tau_6 - \frac{1}{2}g_m\tau_6^2 - \frac{a}{\bar{\omega}^2}\{\cos(|\Psi| - \bar{\omega}\tau_6) - \cos|\Psi|\}$$
$$y_r(\tau_6) = y_5 + \left(v_{y5} + \frac{as_1}{\bar{\omega}}\cos|\Psi|\right)\tau_6 + \frac{as_1}{\bar{\omega}^2}(\sin(|\Psi| - \bar{\omega}\tau_6) - \sin|\Psi|),$$
$$(\tau_6 = t - t_{f1} - 3\delta t - t_a - t_d).$$

Step 7: Altitude adjustment ($t_{f1} + 4\delta t + t_a + t_d < t$)

If there is no error and the lander follows the reference trajectory precisely, it will arrive at the switching altitude to the next subphase at the objective point. However, there are always guidance and control errors which can cause the lander be above the switching altitude at the final point of the subphase. This step is therefore introduced to compensate this. The lander is expected to descend vertically to the altitude of x_6 with a con-

stant velocity v_{x6}.

$$\begin{aligned}
&\psi_r(\tau_7) = 0,\\
&R_r(\tau_7) = 0,\\
&v_{x,r}(\tau_7) = v_{x6},\\
&v_{y,r}(\tau_7) = v_{y6} = 0,\\
&x_r(\tau_7) = x_6,\\
&y_r(\tau_7) = y_6,\\
&\quad(\tau_7 = t - t_{f1} - 4\delta t - t_a - t_d)
\end{aligned}$$

where (v_{x6}, v_{y6}) and (x_6, y_6) are reference velocity and position at the end of the Step 6.

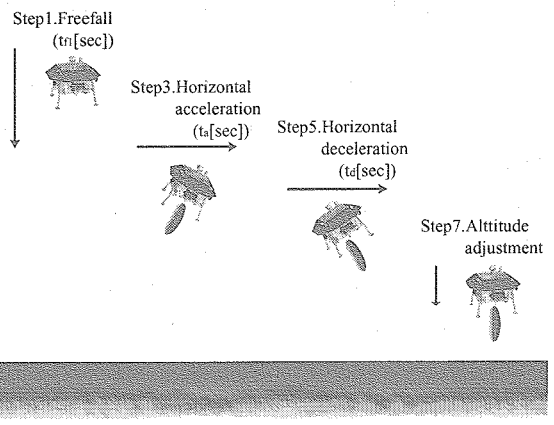

Figure 3: The sequence of the reference trajectory type 1. Transition steps are omitted in this figure.

Trajectory type 2: horizontal deceleration only At the start of the subphase, the lander freefalls (t_{f1} sec), then decelerates horizontally (t_d sec). It then freefalls again (t_{f2} sec), then decelerates vertically (t_{dv}). The direction of deceleration depends on the initial and final horizontal velocities. Let s_2 denote

$$s_2 = \mathrm{sign}(v_{xf} - v_{xi}). \tag{7}$$

Step 1: Freefall ($t \le t_{f1}$)

$$\begin{aligned}
&\psi_r(t) = 0,\\
&R_r(t) = 0,\\
&v_{x,r}(t) = v_{xi} - g_m t,\\
&v_{y,r}(t) = v_{yi},\\
&x_r(t) = x_i + v_{xi}t - \frac{1}{2}g_m t^2,\\
&y_r(t) = y_i + v_{yi}t.
\end{aligned}$$

Step 2: Transition to horizontal deceleration ($t_{f1} \le t \le t_{f1} + \delta t$)

$$\begin{aligned}
&\psi_r(\tau_2) = s_2\bar{\omega}t,\\
&R_r(\tau_2) = s_2\bar{\omega},\\
&v_{x,r}(\tau_2) = v_{x1} - g_m\tau_2 + \frac{a}{\bar{\omega}}\sin(\bar{\omega}\tau_2),\\
&v_{y,r}(\tau_2) = v_{y1} + \frac{as_2}{\bar{\omega}}(1 - \cos\bar{\omega}\tau_2),\\
&x_r(\tau_2) = x_1 + v_{x1}\tau_2 - \frac{1}{2}g_m\tau_2^2 + \frac{a}{\bar{\omega}^2}(1 - \cos\bar{\omega}\tau_2),\\
&y_r(\tau_2) = y_1 + \left(v_{y1} + \frac{as_2}{\bar{\omega}}\right)\tau_2 - \frac{as_2}{\bar{\omega}^2}\sin\bar{\omega}\tau_2,\\
&\quad(\tau_2 = t - t_{f1}).
\end{aligned}$$

Step 3: Horizontal deceleration ($t_{f1} + \delta t \le t \le t_{f1} + \delta t + t_d$)

$$\begin{aligned}
&\psi_r(\tau_3) = \Psi,\\
&R_r(\tau_3) = 0,\\
&v_{x,r}(\tau_3) = v_{x2} + (a\cos\Psi - g_m)\tau_3,\\
&v_{y,r}(\tau_3) = v_{y2} + as_2\sin(|\Psi|)\tau_3,\\
&x_r(\tau_3) = x_2 + v_{x2}\tau_3 + \frac{1}{2}(a\cos\Psi - g_m)\tau_3^2,\\
&y_r(\tau_3) = y_2 + v_{y2}\tau_3 + \frac{1}{2}as_2\sin(|\Psi|)\tau_3^2,\\
&\quad(\tau_3 = t - t_{f1} - \delta t).
\end{aligned}$$

Step 4: Transition to freefall ($t_{f1} + \delta t + t_d \le t \le t_{f1} + 2\delta t + t_d$)

The lander stops horizontal deceleration and returns to vertical attitude with constant angular velocity $-\bar{\omega}$ [rad/sec].

$$\begin{aligned}
&\psi_r(\tau_4) = s_2(|\Psi| - \bar{\omega}\tau_4),\\
&R_r(\tau_4) = -s_2\bar{\omega},\\
&v_{x,r}(\tau_4) = v_{x3} - g_m\tau_4 - \frac{a}{\bar{\omega}}\{\sin(|\Psi| - \bar{\omega}\tau_4) - \sin|\Psi|\},\\
&v_{y,r}(\tau_4) = v_{y3} + \frac{as_2}{\bar{\omega}}\{\cos(|\Psi| - \bar{\omega}\tau_4) - \cos|\Psi|\},\\
&x_r(\tau_4) = x_3 + \left(v_{x3} + \frac{a}{\bar{\omega}}\sin|\Psi|\right)\tau_4 - \frac{1}{2}g_m\tau_4^2\\
&\qquad - \frac{a}{\bar{\omega}^2}\{\cos(|\Psi| - \bar{\omega}\tau_4) - \cos|\Psi|\},\\
&y_r(\tau_4) = y_3 + \left(v_{y3} - \frac{as_2}{\bar{\omega}}\cos|\Psi|\right)\tau_4\\
&\qquad - \frac{as_2}{\bar{\omega}^2}\{\sin(|\Psi| - \bar{\omega}\tau_4) - \sin|\Psi|\},\\
&\quad(\tau_4 = t - t_{f1} - \delta t - t_d).
\end{aligned}$$

Step 5: Secondary freefall ($t_{f1} + 2\delta t + t_d \le t \le t_{f1} + 2\delta t + t_d + t_{f2}$)

The lander freefalls again for t_{f2} seconds, again.

$$\begin{aligned}
&\psi_r(\tau_5) = 0,\\
&R_r(\tau_5) = 0,\\
&v_{x,r}(\tau_5) = v_{x4} - g_m\tau_5,\\
&v_{y,r}(\tau_5) = v_{y4},\\
&x_r(\tau_5) = x_4 + v_{x4}\tau_5 - \frac{1}{2}g_m\tau_5^2,\\
&y_r(\tau_5) = y_4 + v_{y4}\tau_5,\\
&\quad(\tau_5 = t - t_{f1} - 2\delta t - t_d).
\end{aligned}$$

Step 6: Vertical deceleration ($t_{f1}+2\delta t+t_d+t_{f2}\le t\le t_{f1}+2\delta t+t_d+t_{f2}+t_{dv}$)

The lander vertically decelerates for t_{dv} seconds.

$$\begin{aligned}
\psi_r(\tau_6) &= 0,\\
R_r(\tau_2) &= 0,\\
v_{x,r}(\tau_6) &= v_{x5}+(a-g_m)\tau_6,\\
v_{y,r}(\tau_6) &= v_{y5},\\
x_r(\tau_6) &= x_5+v_{x5}\tau_6+\frac{1}{2}(a-g_m)\tau_6^2,\\
y_r(\tau_6) &= y_5+v_{y5}\tau_6,\\
&\quad(\tau_5=t-t_{f1}-2\delta t-t_d).
\end{aligned}$$

Step 7: Altitude adjustment ($t_{f1}+2\delta t+t_d+t_{f2}+t_{dv}<t$)

$$\begin{aligned}
\psi_r(\tau_7) &= 0,\\
R_r(\tau_7) &= 0,\\
v_{x,r}(\tau_7) &= v_{x6},\\
v_{y,r}(\tau_7) &= v_{y6}=0,\\
x_r(\tau_7) &= x_6,\\
y_r(\tau_7) &= y_6,\\
&\quad(\tau_7 = t-t_{f1}-2\delta t-t_d-t_{f2}-t_{dv}).
\end{aligned}$$

3.3.3 Increasing Computational Efficiency

Determining the reference trajectory If there is no error, the lander reaches the switching altitude to the next subphase at the end of step 6 for both types of trajectory. The boundary conditions for step 6 are as follows:

$$\begin{aligned}
v_{x6} &= v_{xf},\quad v_{y6}=v_{yf}=0\\
x_6 &= x_f,\quad y_6=y_f\ ,
\end{aligned}$$

where v_{yf}, x_f, y_f are set according to the subphase or are obtained from the obstacle detection system. For four boundary conditions, we have six unknown parameters of t_{f1}, t_a, t_d, Ψ, α, v_{xf} for the type 1 trajectory type 1 and seven parameters of t_{f1}, t_d, t_{f2}, t_{dv}, Ψ, α, v_{xf} for trajectory type 2. Since the number of unknown parameters is greater than the number of conditions, we can minimize fuel consumption in both cases. We have the following relationships for mass flow

$$\begin{aligned}
\dot{m} &= -\frac{T}{I_{SP}g}=-\frac{T_{\max}u_T}{I_{SP}g}=-\alpha m\\
\Leftrightarrow m &= m_0e^{-\alpha t},\ (u_T:\text{thrust duty cycle})
\end{aligned}$$

so the fuel consumption in the current subphase is

$$\Delta m=m_0(1-e^{-\alpha\Delta t}), \tag{8}$$

where

$$\Delta t=\begin{cases} t_a+t_d+\frac{4\Psi}{\omega} & \text{(type 1)}\\ t_d+t_{dv}+\frac{2\Psi}{\omega} & \text{(type 2)}\end{cases}.$$

As mentioned above, the reference trajectory is determined by choosing parameters to minimize the fuel consumption.

Determination of descent velocity at subphase change The optimization problem is solved numerically to generate the reference trajectory. In this study, Sequential Quadratic Programming (SQP) method [10] is applied to solve this optimization problem. The computer program of SQP method is provided in Matlab toolbox[1].

The amount of computation required for this optimization depends greatly on the number of unknown parameters. Accordingly, the descent velocity at the end of each subphase should be determined by off-line optimization to fix one of unknown parameters beforehand.

When the reference trajectory is generated, the horizontal travel distance to avoid obstacles in the next subphase is unknown. Therefore, the initial descent velocity for the next subphase, which is the final descent velocity for the current subphase, is determined *a priori* by the following approach. The final horizontal velocity is assumed to be 0, and the horizontal travel distance in the next subphase is assumed to be the maximum estimated distance corresponding to 3σ. Since the horizontal velocity is 0 m/s, the reference trajectory is assumed to be type 1. The mass of the vehicle is assumed to be the maximum estimate, which is the severest condition for fuel consumption. Under these assumptions, the final descent velocity for the current subphase is optimized in order to minimize the fuel consumption. This is typical min-max problem approach.

Table 2 shows the conditions and the optimal initial descent velocity for the rough obstacle avoidance and precise obstacle avoidance subphases. From this result, the final descent velocity v_{xf} for the navigation error ac-

Table 2: Appropriate initial descending velocity and subphase conditions

subphase	rough	precise
initial altitude	500m	100m
initial mass	540kg	520kg
horizontal velocity	0m/s	0m/s
travel distance	290m	20m
final altitude	100m	10m
initial descending velocity	13m/s	6m/s

[1](c) Mathworks

commodation and approximate obstacle avoidance subphases are 13 m/s and 6 m/s respectively.

Reachable range In this problem, there is a typical optimization problem difficulty in generating the reference trajectory, namely the large influence of the initial solution on the success of solving the problem. In our approach, the reachable range under the current condition is investigated and it is used to generate the initial solution.

Each of the following cases is investigated to survey the reachable range:

1. Trajectory type 1, $\psi_r > 0$
2. Trajectory type 1, $\psi_r < 0$
3. Trajectory type 2

Maximization and minimization of y_6 is conducted for each case. Each set of maximum and minimum value defines the range where the spacecraft can reach in the case (Figure 4). If the travel distance exists within one of these reachable ranges, the initial solution is set to be one of the boundary value and the optimization problem is solved to generate the reference trajectory. Since case 1 and case 2 never covers the same region, the travel distance can exist within two reachable ranges. In this circumstance, the optimization problem is solved for each cases. This optimization problem has the desirable characteristic that y_6 in each problem changes with respect to ψ and converges easily. Thus, we can achieve the reachable range under the boundary conditions, and we can easily choose the initial solution with appropriate sign of ψ and the reference trajectory is obtained in short time, even if the optimization problem is solved twice. As a result of this approach, we can obtain a reference trajectory in almost all cases, and if the required travel distance does not lie within the reachable range, the closest point is chosen as a feasible value of y_6.

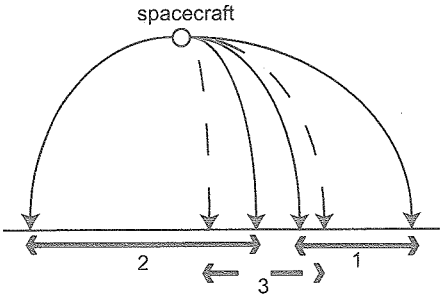

Figure 4: Reachable range by these cases

3.4 Guidance to the Reference Trajectory

This module calculates commands for the main thrust and attitude control, which enables the lander to follow the reference trajectory. It consists of two parts: "calculation of the current reference states" and "guidance."

3.4.1 Calculation of the Current Reference States

In this part, the current reference states (reference position and velocity) are calculated using elapsed time and parameters of the reference trajectory which are obtained from "subphase management" module. Current reference position and velocity can be obtained based on the equation of motion in the reference trajectory coordinates. They are transformed to the lunar local coordinate by C_g^l, and used in the next part.

3.4.2 Guidance

The thrust, angular velocity and attitude commands are calculated by the following steps:

- Calculate nominal forces along each axis of the lunar local coordinate system ($F_{x,r}^l$, $F_{y,r}^l$, $F_{z,r}^l$) using the current reference states.
- The differences between the reference and current states are multiplied by some gains and fed back to the forces $F_{x,r}^l$, $F_{y,r}^l$ and $F_{z,r}^l$.
- Calculate thrust and attitude commands to achieve the calculated command forces $F_{*,a}^l$. If it is impossible to achieve all $F_{*,a}^l$s because of attitude or thrust command limits, compromise solutions are chosen.

First, nominal forces are calculated using the ϕ_g (defined in (3)), ψ_r and a obtained from the reference trajectory generation module and the estimated mass m_e obtained from the mass estimation module.

$$\begin{bmatrix} F_{x,r}^l \\ F_{y,r}^l \\ F_{z,r}^l \end{bmatrix} = C_g^l \begin{bmatrix} \cos\psi_r & -\sin\psi_r & 0 \\ \sin\psi_r & \cos\psi_r & 0 \\ 0 & 0 & 1 \end{bmatrix} \begin{bmatrix} T \\ 0 \\ 0 \end{bmatrix} = \begin{bmatrix} \cos\psi_r \\ \cos\phi_g \cdot \sin\psi_r \\ \sin\phi_g \cdot \sin\psi_r \end{bmatrix} T \tag{9}$$

$$= \begin{bmatrix} \cos\psi_r \\ \cos\phi_g \cdot \sin\psi_r \\ \sin\phi_g \cdot \sin\psi_r \end{bmatrix} \alpha \cdot m_e \cdot I_{SP} \cdot g,$$

where C_g^l is the transformation matrix from the reference trajectory coordinate system to the lunar local coordinate system defined in (2). Feedback terms are added to the nominal forces as follows:

$$F_{x,a}^l = \max\{0,\ F_{x,r}^l + \mathcal{FB}_x\} \tag{10}$$

$$F_{y,a}^l = \begin{cases} 0, & \text{if } F_{y,r}^l \cdot (F_{y,r}^l + \mathcal{FB}_y) < 0, \\ F_{y,r}^l + \mathcal{FB}_y, & \text{otherwise}, \end{cases} \tag{11}$$

$$F_{z,a}^l = \begin{cases} 0, & \text{if } F_{z,r}^l \cdot (F_{z,r}^l + \mathcal{FB}_z) < 0, \\ F_{z,r}^l + \mathcal{FB}_z, & \text{otherwise}, \end{cases} \tag{12}$$

$$\left(\text{where } \begin{array}{l} \mathcal{FB}_x = (K_v \Delta v_x + K_p \Delta x) m_e \\ \mathcal{FB}_y = (K_v \Delta v_y + K_p \Delta y) m_e \\ \mathcal{FB}_z = (K_v \Delta v_z + K_p \Delta z) m_e \\ \Delta v_* = v_{*,r}^l - v_*^l,\ \Delta * = *_r^l - *^l \end{array} \right),$$

where

v_*^l : current velocity
$*^l$: current position
$v_{*,r}^l$: current reference velocity
$*_r^l$: current reference position
(in the lunar local coordinate system).

$F_{x,a}^l$ is always greater than zero since the main thruster does not have a gimbal mechanism. Note that if the signs of $F_{*,r}^l$ and $F_{*,a}^l$ differ after adding feedback terms $\mathcal{FB}_*$, $F_{y,a}^l$ and $F_{z,a}^l$ are set to zero in order to prevent oscillatory behavior around the reference trajectory.

Command inputs uT_a, θ_a and ψ_a are calculated to realize the $F_{*,a}^l$.

$$C_a^l(\phi_a, \theta_a, \psi_a) \begin{bmatrix} T_{\max} \cdot uT_a \\ 0 \\ 0 \end{bmatrix} = \begin{bmatrix} F_{x,a}^l \\ F_{y,a}^l \\ F_{z,a}^l \end{bmatrix}. \tag{13}$$

In this study we suppose that the lander does not rotate about its x axis. The command input ϕ_a is fixed at the initial roll angle ϕ_i.

Case A: if $\alpha = 0$ This means the reference thrust is zero, that is, the lander is at the "freefall" step. In this case,

$$\begin{aligned} uT_a &= 0, \\ \phi_a &= \phi_i, \\ \theta_a &= 0, \\ \psi_a &= 0, \\ P_a = 0,\ Q_a &= 0,\ R_a = 0, \end{aligned}$$

where P_a, Q_a, R_a are roll, pitch, yaw angular velocity commands respectively.

Case B: if $F_{x,a}^l = 0$ It is impossible to realize $F_{y,a}^l$ and $F_{z,a}^l$ without excess of angles. Thus, uT_a should be zero and reference angles should be used as command inputs:

$$\begin{aligned} uT_a &= 0, \\ C_b^l(\phi_a, \theta_a, \psi_a) &= \begin{bmatrix} \cos\psi_r \\ \cos\phi_g \cdot \sin\psi_r \\ \sin\phi_g \cdot \sin\psi_r \end{bmatrix}. \end{aligned}$$

$$\Leftrightarrow \begin{cases} \phi_a = \phi_i, \\ \theta_a = \tan^{-1}\{\sin\psi_r \sin\phi_a - \sin\phi_g \tan\psi_r \cos\phi_a\}, \\ \psi_a = \sin^{-1}\{\cos\phi_g \sin\psi_r \cos\phi_a + \sin\phi_g \sin\psi_r \sin\phi_a\}, \end{cases}$$

$$\begin{bmatrix} P_a \\ Q_a \\ R_a \end{bmatrix} = C_l^a(\phi_a, \theta_a, \psi_a) \cdot C_g^l(\phi_g) \begin{bmatrix} 0 \\ 0 \\ R_r \end{bmatrix},$$

$$(C_l^a = \{C_a^l\}^{-1}).$$

Note that the angular velocity commands should be defined in the target attitude coordinates.

Case C: otherwise Calculate the command inputs using $F_{*,a}^l$:

$$\begin{aligned} \phi_a &= \phi_i \\ \theta_a &= \tan^{-1}\left\{\frac{F_{y,a}^l \sin\phi_a - F_{z,a}^l \cos\phi_a}{F_{x,a}^l}\right\}, \\ \psi_a &= \tan^{-1}\left\{\frac{(F_{y,a}^l \cos\phi_a + F_{z,a}^l \sin\phi_a) \cdot \cos\theta_a}{F_{x,a}^l}\right\}, \\ uT_a &= \frac{F_x^l}{T_{\max} \cos\theta_a \cos\psi_a}, \\ \begin{bmatrix} P_a \\ Q_a \\ R_a \end{bmatrix} &= C_l^a(\phi_a, \theta_a, \psi_a) \cdot C_g^l(\phi_g) \begin{bmatrix} 0 \\ 0 \\ R_r \end{bmatrix}. \end{aligned}$$

If some of the commands exceed the limits, that is, $\theta_a > \theta_{\max}$ or $\psi_a > \psi_{\max}$ or $uT_a > 1$, these should be re-calculated as follows:

- If $F_{x,a}^l > T_{\max} \cos\theta_{\max} \cos\psi_{\max}$
  $F_{x,a}^l$ cannot be realized within the limits in this case. Thus uT_a should be set to be 1 to maximize F_x^l. Attitude commands, θ_a and ψ_a, should be calculated again.

$$\begin{aligned} uT_a &= 1, \\ \psi_a &= \begin{cases} \psi_{\max} \cdot \text{sign}(\mathcal{R}_y), & \text{if } \left|\sin^{-1}\mathcal{R}_y\right| > \psi_{\max}, \\ \sin^{-1}\mathcal{R}_y, & \text{otherwise}, \end{cases} \\ \theta_a &= \begin{cases} \theta_{\max} \cdot \text{sign}(\mathcal{R}_z), & \text{if } \left|\sin^{-1}\mathcal{R}_z\right| > \theta_{\max}, \\ \sin^{-1}\mathcal{R}_z, & \text{otherwise}, \end{cases} \end{aligned}$$

where $\mathcal{R}_y = \dfrac{F^l_{y,a}\cos\phi_a + F^l_{z,a}\sin\phi_a}{T_{\max}}$,

$\mathcal{R}_z = \dfrac{F^l_{y,a}\sin\phi_a - F^l_{z,a}\cos\phi_a}{T_{\max}\cdot\cos\psi_a}$.

- Otherwise

  Either $F^l_{y,a}$ or $F^l_{z,a}$ (or both) cannot be realized. In this case, the command inputs are re-calculated so that F^l_y and F^l_z are maximized within the limits with keeping $F^l_x \approx F^l_{x,a}$.

$$\theta_a = \begin{cases} \theta_{\max}\cdot\mathrm{sign}(\mathcal{R}_z), & \text{if } \left|\tan^{-1}\mathcal{R}_z\right| > \theta_{\max}, \\ \tan^{-1}\mathcal{R}_z, & \text{otherwise}, \end{cases}$$

$$\psi_a = \begin{cases} \psi_{\max}\cdot\mathrm{sign}(\mathcal{R}_y), & \text{if } \left|\tan^{-1}\mathcal{R}_y\right| > \psi_{\max}, \\ \tan^{-1}\mathcal{R}_y, & \text{otherwise}, \end{cases}$$

$$uT_a = \frac{F^l_{x,a}}{T_{\max}\cos\theta_a\cos\psi_a},$$

where $\mathcal{R}_y = \dfrac{F^l_{y,a}\cos\phi_a + F^l_{z,a}\sin\phi_a}{F^l_{x,a}}\cos\theta_a$,

$\mathcal{R}_z = \dfrac{F^l_{z,a}\cos\phi_a - F^l_{y,a}\sin\phi_a}{F^l_{x,a}}$.

3.5 Main Thrust Modulation

Although the main thruster in this study operates only in a pulse mode (simple on-off), almost arbitrary thrust levels can be achieved by modulating the width of the activation pulses proportionally to the magnitude of the thrust command input (so-called pulse width modulation (PWM)). In this case, the minimum on-time and off-time of the thruster are greater than the sampling period of the guidance system. Thus, modulation is applied so that the average thrust within several sampling periods approximates the thrust command input.

This module is composed of two parts depicted in Figure 5. In the "pulse calculator" part, on-time and off-time of a pulse is calculated based on the thrust command input, and the pulse is generated in the "pulse generator" part. The pulse generator outputs "1" for the time of t_{on} seconds and outputs "0" for the time of t_{off} seconds. After outputting "0", it triggers the pulse calculator.

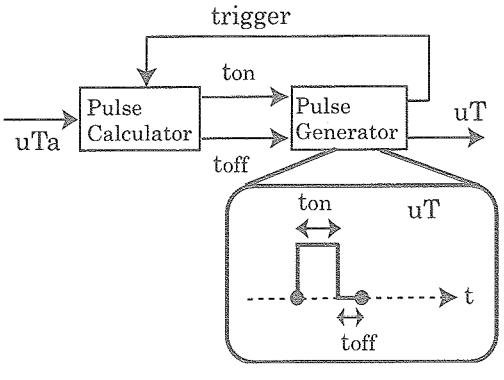

Figure 5: The "main thrust modulation" module and generated pulse.

3.5.1 Pulse Calculator

This calculates on-time and off-time of an output pulse according to the level of the thrust command input uT_a. The minimum on-time ($Ton_{\min}$) and off-time ($Toff_{\min}$) of the thruster should be considered in the calculation.

- $uT_a \le \frac{Ton_{\min}}{Ton_{\min}+2\times Toff_{\min}}$

  In order to achieve the thrust level uT_a on an average, more than ($Ton_{\min} + 2 \times Toff_{\min}$) seconds are necessary, which is too long compared to the sampling period. Thus the pulse is not generated (t_{on} = 0, t_{off} = $Toff_{\min}$) and the current value of uT_a is carried forward to the next period's value to prevent lack of the thrust.

- $\frac{Ton_{\min}}{Ton_{\min}+2\times Toff_{\min}} < uT_a \le \frac{Ton_{\min}}{Ton_{\min}+\times Toff_{\min}}$

  In this case, t_{on} is fixed at $Ton_{\min}$ and t_{off} is calculated so as to achieve the thrust command level uT_a:

$$t_{off} = Ton_{\min}\times\frac{1-uT_a}{uT_a}.$$

  Using the calculated t_{off}, the output uT approximates the thrust command level on the average.

- $\frac{Ton_{\min}}{Ton_{\min}+Toff_{\min}} < uT_a \le \frac{2\times Ton_{\min}}{2\times Ton_{\min}+\times Toff_{\min}}$

  As opposed to the previous case, t_{off} is fixed at $Toff_{\min}$ and ton is calculated as follows:

$$t_{on} = Toff_{\min}\times\frac{uT_a}{1-uT_a}.$$

- $\frac{2\times Ton_{\min}}{2\times Ton_{\min}+Toff_{\min}} < uT_a$

  Since more than ($2 \times Ton_{\min} + Toff_{\min}$) seconds, which is too long compared to the guidance cycle, are necessary to achieve the thrust command level, t_{on} is set at $Ton_{\min}$. Although this may cause excessive thrust, it is not a problem for safe landing.

3.5.2 Pulse Generator

The pulse command uT is generated during the time of ($t_{on} + t_{off}$) seconds. The elapsed time from the beginning of the pulse command is counted by the pulse counter. The initial value of the counter is zero. When it counts ($t_{on} + t_{off}$) seconds, it is reset and the pulse calculator part is

triggered.

3.6 Attitude Control

This module calculates RCS torques from commands, current angles and angluar velocities[2]:

$$\begin{aligned} T_r &= Kp_r(\phi_a - \phi) + Kd_r(P_a - P), \\ T_p &= Kp_p(\theta_a - \theta) + Kd_p(Q_a - Q), \\ T_y &= Kp_y(\psi_a - \psi) + Kd_y(R_a - R), \end{aligned} \tag{14}$$

where P, Q and R are current angular velocities.

3.7 Mass Estimation

This module estimates the current mass of the lander. The fuel consumption rate is calculated as:

$$\frac{dm}{dt} = -\frac{T}{g \cdot I_{SP}} = -\frac{T_{\max} \cdot uT}{g \cdot I_{SP}}.$$

Therefore, the mass is estimated by the following equation:

$$m_e = m_0 - \int_0^t \frac{T_{\max} \cdot uT}{g \cdot I_{SP}} dt. \tag{15}$$

4. Monte Carlo Simulation with the Nominal Configuration

4.1 Types of Uncertainties

Monte Carlo simulations of lunar landing were conducted to validate the guidance and control system and to evaluate its robustness against uncertainty. Various uncertain parameters and their distributions are assumed in the simulation. Table 3 shows the uncertain parameters considered here. Parameter values are generated randomly with their assumed distributions at each iteration. Apart from these parameters, small random noise is also included in the IMU and RA/RV outputs.

4.2 Success Criteria

The landing experiment has two main objectives:

- precise landing at the target site,
- safe landing on the moon.

The lander should achieve the mission success criterion for each objective.

[2]The RCS is assumed to generate desirable torque with some delay in this simulation.

Table 3: Uncertain parameters in Monte Carlo simulation (1σ value).

Sensor		
IMU (1: accelerometer) (2: gyro)	Bias Error	60.0[μG][1] 0.005[deg/hr][2]
	Scale Factor	100.0[ppm][1] 6.0[ppm][2]
	Miss Alignment	200.0[μrad][1,2]
	Random Walk	0.01[deg/hr$^{1/2}$][2]
RA/RV (3: RA) (4: RV)	Bias Error	0.5[m][3] 0.2[m/sec][4]
	Scale Factor	0.5[%][3,4]
	Miss Alignment	200.0[μrad][3,4]
Obstacle Detection	Scale Factor	1.0[%]
	Miss Alignment	1.0[deg]
	Objective Point	68.354[m][5] 4.714[m][6]
(5: Rough avoidance subphase, 6: Precise avoidance subphase)		

Lander Model		
Thruster (7: Thrust) (8: I_{SP})	Bias Error	10.0[N][7] 0.6667[kgf・sec/kg][8]
	Scale Factor	1.5[%][7,8]
	Miss Alignment	0.5[deg]

Environment		
Gravitational Acceleration	Bias Error	0.001[m/sec^2]

Initial Condition		
State Variables	Position	0.0[m][9] 117.851[m][10]
	Velocity	0.0[m/sec][9,10]
	Mass	10.0[kg]
Initial Navigation Error	Position	10.0[m][9] 6.0[m][10]
	Velocity	0.4[m][9,10]
	Attitude	0.013[arcmin]
(9: Altitude, 10: East & North)		

4.2.1 Precise Landing

An initial navigation error exists at the beginning of the vertical descent phase. Since the lander is required to land at an obstacle-free area in the vicinity of the target site, it must be in a position where the obstacle detection system can capture the target site at the beginning of the rough obstacle avoidance subphase. Since the angle of view of the obstacle detection system's stereo cameras is 30 degrees, the success criterion is as follows:

Criterion-1 Horizontal position error is less than 134 meters ($=\tan\frac{30^\circ}{2}\times 500$) at the start of the rough obstacle avoidance subphase.

4.2.2 Safe Landing

In the simulation, the central peak of a crater and a lava dome in the lunar highlands are supposed to be the leading candidates for a target site. It has been proved in our previous study [9] that around these regions there is at least one 10m × 10m or wider obstacle-free square area within a distance of 325m, which is the maximum side shift achievable after the rough and precise obstacle avoidance subphases.

Considering the size of the lander is about 4m and the fact that the obstacle detection system can detect a safety area of 10m × 10m (or wider), we obtain Criterion-2 as follows:

Criterion-2 Horizontal position error at touchdown is less than 3m (= (10 − 4)/2).

Added to these are the following criteria mentioned in section 2:

Criterion-3 The maximum descent velocity at touchdown is 3m/s, and

Criterion-4 The main thruster is cut-off above 2m.

4.3 Simulation Results

A Monte Carlo simulation was carried out with 1,000 iterations. Figure 6-9 show the results, which are also summarized in Table 4.

The distribution of the position error at the start of rough obstacle avoidance subphase is shown in Fig. 6. The mean value of the error is 51.67m and the 3σ value is 79.38m. The error exceeds 134m in only three cases out of 1,000. Figure 7 shows position error at touchdown. The mean value of the error is 11.03m and the 3σ value is 17.69m. It follows from these results that **Criterion-1** is satisfied and precise landing within 30m of the objective point is achievable.

However, for **Criterion-2**, the position error at touchdown exceeds the 3m limit in 942 cases. Furthermore,

Table 4: Simulation results.

Parameter	Mean value	1 σ
Position error*1	51.67[m]	26.46[m]
Position error*2	11.04[m]	5.897[m]
Guidance error*2	0.2537[m]	0.1378[m]
Descending velocity*2	3.017[m/s]	1.199[m/s]
Horizontal velocity*2	0.3960[m/s]	0.2129[m/s]
Last pulse	2.788[m]	2.661[m]
Fuel consumption	57.60[kg]	2.161[kg]

*1: at the beginning of rough avoidance subphase.
*2: at touchdown.

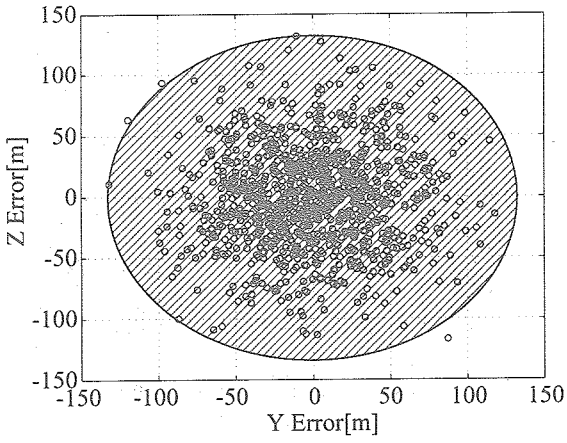

Figure 6: Distribution of position error at the start of the rough obstacle avoidance subphase. The magnitude is within 134[m] in 997 cases.

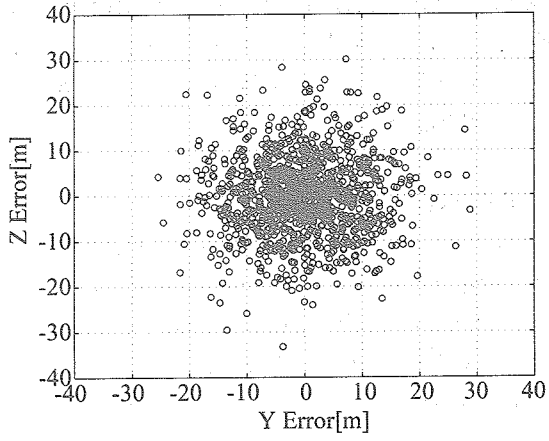

Figure 7: Distribution of position error at touchdown. The magnitude is within 3[m] in 58 cases.

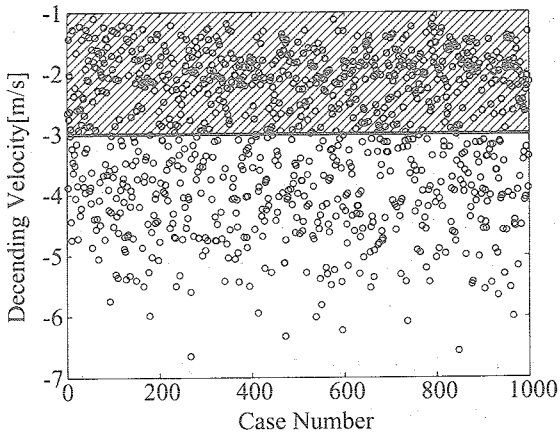

Figure 8: Distribution of descent velocity at touchdown. The velocity is within 3[m/s] in 531 cases.

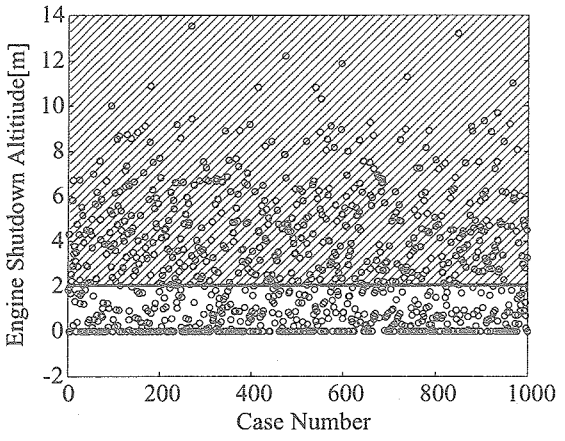

Figure 9: Distribution of altitude of the main engine shutdown. It is above 2[m] in 521 cases.

Criterion-3 and **Criterion-4** fail to be satisfied in almost half of the cases. The descent velocity exceeds the limit in 469 cases (Fig. 8), as does the altitude of main engine cut-off in 479 cases (Fig. 9).

4.4 Discussion

Since the RA/RV is not available below 30m, the accuracy of the integrated navigation deteriorates at lower altitude. Considering the fact that the mean value of the guidance error at touchdown is 0.2537m, it is thought that excessive position error is caused mainly by navigation error. It follows that the lander needs to be equipped with another altimeter and velocimeter for lower altitudes in order to reduce the position error, or the landing sequence needs to be changed so that the lander can avoid all obstacles above 30m. If these are impossible, the target site should be changed to a flat area where distribution of obstacles is less than that considered in this paper.

For **Criterion-3** and **Criterion-4**, since the mean value of descent velocity at the last thrust pulse is 1.202m/s, exceedences of the limits are supposed to be caused by altitude error. If the main thruster can stop exactly at an altitude of 2m, the touchdown velocity is expected to be less than 3m/s. One possible way to achieve this is to equip the lander with a 2m-long lunar surface-sensing probe that will trigger main thruster cut-off, as in the case of the Apollo Lunar Module, which had a 5-foot probe.

5. Monte Carlo Simulation with the Modified Configuration

The lander configuration and landing sequence are modified based on the discussion as in the following subsection. A Monte Carlo simulation is carried out again with 1,000 iterations using the same uncertain parameters and their distributions.

5.1 Modified Lander Configuration and Landing Sequence

- Surface-sensing Probe

  The lander is equipped with a 2m-long lunar surface-sensing probe, which triggers main thruster cut-off to avoid stirring up lunar surface material (regolith) by using the main thruster near the surface. This is similar to the 5-foot probe used by the Apollo Lunar Module.

- Hovering Subphase

  The landing sequence is modified as follows:
  - Initial error accommodation (3,500m-500m altitude)
  - Rough obstacle avoidance (500m-150m)
  - Precise obstacle avoidance (150m-40m)
  - Hovering (around 40m)
  - Constant speed descent (40m-2m)
  - Freefall (2m-0m)

The hovering subphase is introduced to accomodate the horizontal position error accumulated during the precise obstacle avoidance subphase. The lander moves slowly to above the center of the obstacle-free area while maintaining an altitude of around 40m. This altitude is settled considering the fact that the RA/RV is not available below 30m, and the Monte Carlo simulation results which show that the maximum altitude error around 30m is about 10m.

During the hovering subphase, commands are calculated without nominal forces (that is, $F^{l}_{*,a} = \mathcal{FB}_{*}$ in

Table 5: Simulation results with the modified configuration.

Parameter	Mean value	1σ
Position error*1	51.58[m]	26.41[m]
Position error*2	4.021[m]	4.169[m]
Descent velocity*2	2.778[m/s]	0.2369[m/s]
Horizontal velocity*2	0.4190[m/s]	0.3641[m/s]
Last pulse	2.210[m]	0.5444[m]
Fuel consumption	63.55[kg]	3.161[kg]

*1: at the start of rough avoidance subphase.
*2: at touchdown.

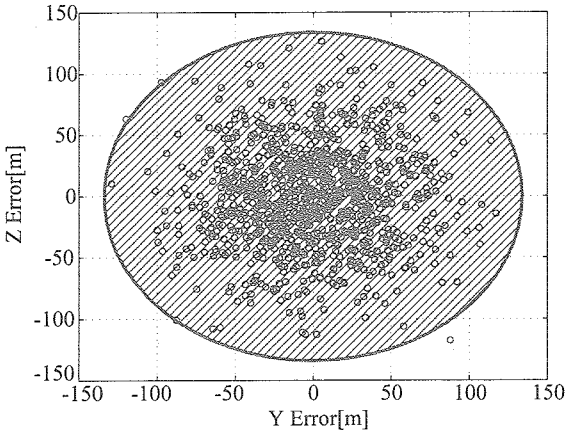

Figure 10: Distribution of position error at the start of the rough obstacle avoidance subphase. The magnitude is within 134[m] in 997 cases.

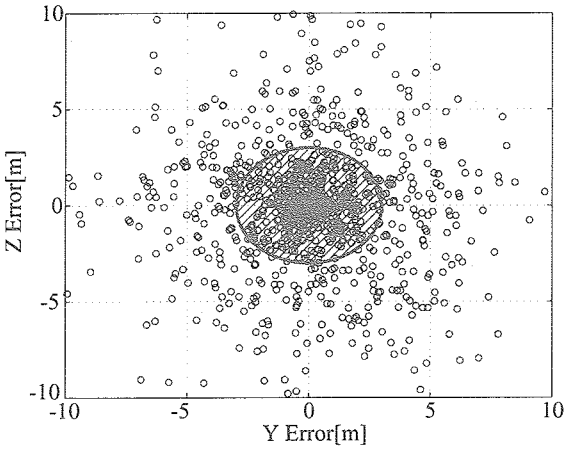

Figure 11: Distribution of position error at touchdown. The magnitude is within 3[m] in 488 cases.

(10) − (12)). The reference altitude x_r^l is set at 40m and the reference descent velocity $v_{x,r}^l$ is set at 0m/s. The reference horizontal velocity varies between -2m/s and +2m/s depending on the horizontal distance to the objective point.

- Obstacle Detection System

  The obstalce detection system is used for estimating relative position between the lander and the obstacle-free area in order to reduce the horizontal position errorfrom the beginning of the hovering subphase. The sampling period of the system is assumed to be one second and it is activated only when the main thruster is not firing.

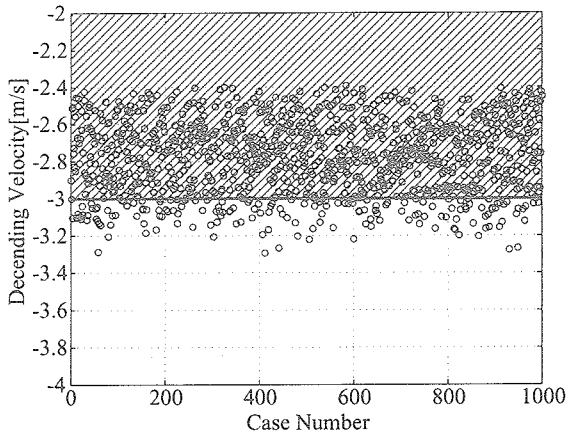

Figure 12: Distribution of descent velocity at touchdown. The velocity is within 3[m/s] in 828 cases.

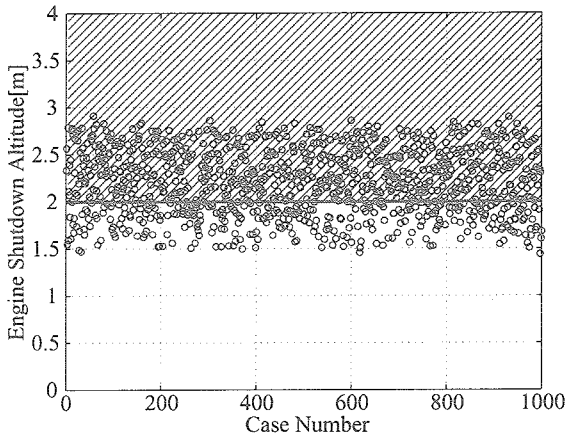

Figure 13: Distribution of altitude of the main engine shutdown. It is above 2[m] in 664 cases.

5.2 Simulation Results

Figure 6-9 show the results of the 1,000 Monte Carlo simulation trials using the modified configuration, which are also summarized in Table 4.

The distribution of position error at the start of rough obstacle avoidance subphase is shown in Fig. 6. The error exceeds 134m in only three cases out of 1,000. It follows from these results that Criterion-1 is satisfied.

Figure 7 shows position error at touchdown. Compared to the SELENE-B configuration in which the error exceeded the 3m limit in 942 cases, the probability of success is obviously improved by the introduction of the hovering subphase. Although fuel consumption is greater compared to the SELENE-B result of 57.60kg, the increase is only a few kilograms and is considered to be acceptable.

The distributions of descent velocity and main engine cut-off altitude are shown in Fig. 8 and 9. Criterion-3 and Criterion-4 are satisfied in 828 cases and 664 cases respectively. The exceedence of the shutdown altitude limit in 336 cases in spite of the lunar surface-sensing probe is considered to be due to the main thruster's response delay to the shut-off command and its minimum on-time.

6. Conclusion

We evaluated a guidance and control system for safe and precise landing on the moon with optimum fuel consumption by Monte Carlo simulation. It was shown that the system with modified configuration can achieve precise landing, and the error at landing is significantly lower compared to the original lander configuration. The main thruster shutdown altitude, however, exceeded its limit in about 34% of cases, and this does not give a satisfactorily high probability of safe landing. The algorithm for shutdown should therefore be modified in consideration of the delay and minimum on-time of the main thruster. Furthermore, position error at landing still failed to satisfy the 3m maximum criterion in almost half of the cases. We are planning to redesign the feedback gains during the hovering subphase in order to improve the results, which will be shown in future studies.

References

[1] "Udaipur Declaration", the sixth International Conference on the Exploration and Utilization of the Moon (2004).

[2] E. C. Aldridge, Jr., "A Journey to Inspire, Innovate, and Discover", Report of the President's Comission on Implementation of United States Space Exploration Policy (2004).

[3] http://www.esa.int/export/SPECIALS/SMART-1/

[4] http://www.jaxa.jp/about/vision_missions/long_term/index_e.html

[5] http://www.isas.jaxa.jp/e/enterp/missions/selene/

[6] SELENE-B Team (ISAS/NAL/NASDA), "Proposal of the SELENE-B Mission" , 2002 (in Japanese).

[7] M. Yamamoto, et al., "Navigation and Guidance Simulation for SELENE-B Lunar Landing" , Proceedings of the 47th Space Sciences and Technology Conference, pp.174-179, 2003 (in Japanese).

[8] Y. Hamada, T. Ninomiya, S. Sasa, Y. Shinomiya, S. Ueno, Y. Ishijima, M. Yamamoto and S. Sawai, "A Study on SELENE-B Guidance and Control System for Pin-point Lunar Landing" , Proceedings of the 47th Space Sciences and Technology Conference, pp.180-185 (2003) (in Japanese).

[9] T. Ninomiya, T. Fujiwara, Y. Hamada, S. Sasa, Y. Ishijima, K. Hayashi, A. Kojima and S. Sawai, "A Study on Navigation, Guidance and Control for Moon Landing" , Proceedings of the 23rd International Symposium on Space Technology and Science, vol. II, pp.1872-1877, (2002).

[10] Fletcher, R., "Practical Methods of Optimization" , John Wiley and Sons (1987).

JAXA Research and Development Report JAXA–RR–05–013E

Date of Issue : December 28, 2005
Edited and Published by : Japan Aerospace Exploration Agency
7-44-1 Jindaiji-higashimachi, Chofu-shi, Tokyo 182-8522, Japan
URL : http://www.jaxa.jp/
Printed by : Kyoushin Co., Ltd.

Japan Aerospace Exploration Agency

Printed on Recycled Paper